Mechanical Technology and Engineering Insights

www.mtei.reapress.com

Mech. Technol. Eng. Insights . Vol. 2, No. 2 (2025) 105–120.

Paper Type: Original Article

Mixed Convection in A Square Cavity with Heat-Generating Conducting Body

Victoria Nozick[1,*], Omar Mar Cornelio[2]

[1] Departmant of Operations and Information Management Group, Aston Business School, Aston University, B4 7ET Birmingham, United Kingdom; victorianozick79@gmail.com.

[2] Centro de Estudio de Matemática Computacional, Universidad de las Ciencias Informáticas, 19370 La Habana, Cuba; omarmar@uci.cu.

Citation:

Received: 21 September 2024 *Revised: 10 November 2024* *Accepted: 18 Januray 2025*	Nozick, V., & Mar Cornelio, O. (2025). Mixed convection in a square cavity with a heat-generating conducting body. *Mechanical Technology and Engineering Insights, 2*(2), 105-120.

Abstract

In this research, a steady mixed convection in a square cavity with a heat-generating conducting body is investigated, where the bottom wall is kept at a constant high temperature of T_h and the top wall is kept at a constant low temperature of T_c, respectively. The left and right side walls are assumed to be insulated. The inlet port of cold air is located on the bottom of the left wall. The fluid properties are assumed to be constant, except for the density in the buoyancy term, which follows Boussinesq's approximation. Continuity, momentum, and energy equations are solved by using a finite volume method and SIMPLE algorithm in which convection terms are applied by using the Power-Law scheme. Results have been compared with published results for two similar cases, where a good agreement is achieved. Positioning the outlet ports at three locations on the right wall for Re = 20, 100, and 300, Ri = 0, 0.5, 1, and 10, and Pr = 0.7, where a total of 36 cases were studied. Results have shown that, for a configuration where the exit port is located at the top of the right wall, and the solid body is situated on the genuine route of the fluid flow from inlet to outlet, cooling of the heat-generating body is optimum. For this case, the vorticity region around the body decreases, where the hot body comes in contact with the incoming cold air jet, decreasing the temperature.

Keywords: Mixed convection, Square cavity, Heat-generating conducting, SIMPLE algorithm.

1 | Introduction

Mixed convection in a cavity with a heat-generating body finds wide industrial applications, such as cooling of electronic devices, room cooling, and chemical processing equipment. In mixed convection, heat transfer in flows in which the influence of forced convection and natural convection are of comparable magnitude. However, the ratio of Gr/Re2 has been used to present the relative magnitudes of forced and natural

Corresponding Author: victorianozick79@gmail.com

https://doi.org/10.48313/mtei.v2i2.43

convection in mixed convection flows. Moreover, mixed convection flows may be further subdivided into those where the inertia force is parallel to the buoyancy force and those where the inertia force is perpendicular to the buoyancy force. A large number of heat-generating devices, which dissipate moderate amounts of heat, are cooled by an external fluid driver such as an air fan. The cooling systems are designed in such a way that the convection due to the air stream and buoyancy-induced natural convection aid each other in the resulting mixed convective heat transfer process.

Efforts must be made to avoid the appearance of isolated recirculation zones carrying hot fluid. A hot recirculation zone, which does not interact with the incoming air jet, may lead to a high temperature field, close to the heat-generating surface. The mixing can be improved, and the amount of heat trapped in these zones can be minimized by carefully choosing the relative locations of the inlet and outlet. Considerable research studies were carried out on natural, forced, and mixed convection heat transfer. Papanicolaou and Jaluria [1] performed computations for applications of electronic equipment cooling with the inlet and outlet placed in vertical walls. For a fixed aspect ratio, Reynolds and Grashof numbers were varied for various locations of the heat source and outlet opening. The numerical study on natural convection in a partitioned cubic enclosure was carried out by Karki et al. [2]. They explored the effects of various parameters on the flow structure and heat transfer. They indicated that the three-dimensional effects were significant for the Rayleigh numbers considered in the study. The combined force and natural convection heat transfer within a recirculation flow in an insulated lid-driven cavity of rectangular cross section was investigated by Prasad and Koseff [3]. The mean heat flux over the entire lower boundary was analyzed, and the correlation for Nusselt and Stanton numbers was developed. They showed that the flow in the cavity was independent of Gr/Re2 over the range studied.

Hsu et al. [4] put a baffle inside the enclosure with two different orientations, with a partition protruding either from the bottom wall or from the top wall. The effect of the baffle and its position on mixed convection was studied. Lee et al. [5] provided finite-element solutions of laminar and turbulent flows with forced and mixed convection in an air-cooled room. Singh and Sharif [6] studied natural convection in enclosures heated from one side and cooled from the ceiling. Omri and Nasrallah [7] studied mixed convection in a rectangular enclosure with differentially heated vertical side walls having openings for inlet and outlet. Two different placement configurations of the inlet and outlet openings on the side walls were investigated.

In the first case, the cold air was injected at the top of the hot wall and exited at the bottom of the cold wall, whereas in the second configuration, the injection was at the lower edge of the hot wall and the exit was at the top of the cold wall. Improvement in cooling efficiency was found with the inlet placed at the bottom of the hot wall. Mixed convection in a rectangular enclosure with discrete heat sources was studied numerically by Hsu and Ang [8]. The computational results indicate that both the thermal field and the average Nusselt number depend strongly on the governing parameters, such as Reynolds number, buoyancy parameter, and position of the heat sources.

Lee et al. [9] studied the problem of natural convection in a square enclosure with isothermal top and bottom boundaries and various conditions of thermal boundary of interior body, and also, the aspect ratio effect of given enclosure with equi-spaced array of bodies. They concluded that the transition of flow from quasi-steady up to unsteady convection depends on the presence of bodies and aspect ratio effect of the cell. In this research, a steady mixed convection in a square cavity with a heat-generating conducting body is numerically analyzed. The bottom wall is kept at a constant high temperature of Th, whereas the top wall is kept at a constant low temperature of Tc, respectively. The left and right side walls are assumed to be insulated. The injection of cold air is considered at the bottom of the left wall. Positioning the outlet ports at three locations on the right wall for a range of Reynolds and Richardson numbers, a total of 36 cases were studied.

2 | Problem Description

A schematic of the system considered in this research is shown in *Fig. 1*. The system consists of a square cavity with sides of length L, within which a rectangular body is centered, where it has a thermal conductivity of ks and a heat generation per unit volume of q. The bottom wall is kept at a constant high temperature of Th, whereas the top wall is kept at a constant low temperature of Tc, respectively. The left and right side walls are assumed to be insulated. The fluid enters the cavity through an inlet port of width Di, which is located at the bottom of the left vertical wall. The widths of the inlet and outlet ports are kept identical (Di = Do). An exit port can be present on any of the three locations on the right wall. A special coordinate system (s) along the right wall is adopted with its origin at x = L and y = L, as identified in *Fig. 1*. Three different configurations have been considered as shown in *Table 1*. The temperature of the fluid entering the cavity is Tin, whereas Tin < Tc.

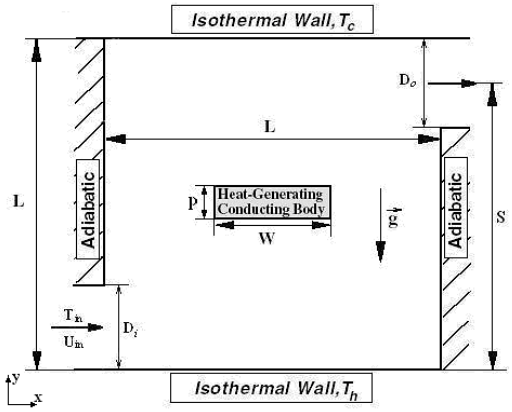

Fig. 1. Schematic diagram of the cavity with a heat-generating body.

Table 1. Location of the exit port on the right wall of the cavity.

Configuration III	Configuration II	Configuration I
0.875	0.5	0.125

3 | Mathematical Modeling

The radiation effects have been assumed to be negligible. The flow is two-dimensional, steady state, laminar, and the fluid properties have been assumed constant, except for the density in the buoyancy term, which follows the Boussinesq approximation. The gravitational acceleration acts in the negative y-direction. Thus, in this study, the fluid flow with a heat-generating conducting body at the center has been considered. Dimensionless form of the governing equations can be obtained by introducing dimensionless variables. The lengths can be scaled by the cavity length L, where the velocities can be scaled by the inlet fluid velocity, uin. As for the temperature, the two extreme values (Tc and Th) are used. The dimensionless variables are then defined as:

$$X = \frac{x}{L},\ Y = \frac{y}{L},\ U = \frac{u}{u_0},\ V = \frac{v}{u_0},\ P = \frac{p}{\rho u_0^2},\ \theta = \frac{T - T_C}{T_H - T_C}. \quad (1)$$

Variables u, v, p, and T are the velocity components in the x-and y-directions, pressure, and temperature, respectively. Based on the dimensionless variables above, the dimensionless equations for the conservation of mass, momentum, and thermal energy are

$$\frac{\partial U}{\partial X} + \frac{\partial V}{\partial Y} = 0. \quad (2)$$

$$U\frac{\partial U}{\partial X}+V\frac{\partial U}{\partial Y}=-\frac{\partial P}{\partial X}+\frac{1}{Re}\left(\frac{\partial^2 U}{\partial X^2}+\frac{\partial^2 U}{\partial Y^2}\right). \quad (3)$$

$$U\frac{\partial V}{\partial X}+V\frac{\partial V}{\partial Y}=-\frac{\partial P}{\partial Y}+\frac{1}{Re}\left(\frac{\partial^2 V}{\partial X^2}+\frac{\partial^2 V}{\partial Y^2}\right)+\frac{Gr}{Re^2}\theta. \quad (4)$$

$$U\frac{\partial \theta}{\partial X}+V\frac{\partial \theta}{\partial Y}=\frac{1}{Re\,Pr}\left(\frac{\partial^2 \theta}{\partial X^2}+\frac{\partial^2 \theta}{\partial Y^2}\right). \quad (5)$$

$$K\left(\frac{\partial^2 \theta}{\partial X^2}+\frac{\partial^2 \theta}{\partial Y^2}\right)+\frac{\Delta T}{A}=0. \quad (6)$$

In the energy equation, the viscous dissipation terms have been neglected. Dimensionless parameters have been defined as:

$$Re=\frac{u_{in}L}{\upsilon},\ Gr=\frac{g\beta L^3(T_h-T_c)}{\nu^2},\ Pr=\frac{\nu}{\alpha},\ A=\frac{WP}{L^2},\ \Delta T=\frac{\dot{q}W^2/k_f}{T_h-T_c},\ k=\frac{k_s}{k_f}. \quad (7)$$

The ratio Gr/Re^2 is known as the Richardson number, Ri, where its value defines the different convection regimes, where for forced convection Ri«1, and for natural convection Ri»1. For the mixed convection case where forced and natural convection are equally dominant, Ri is of the order of 1. The area ratio, A, is taken to be 1/45, where the Prandtl number is taken to be 0.7, corresponding to air. Reynolds and Richardson numbers are varied over the range of 20–300 and 0–10, respectively. The values of temperature difference ratio, ΔT, and the dimensionless thermal conductivity, k, are kept constant at 100 and 20, respectively. No-slip boundary conditions (U=V=0) are used on all the walls. Adiabatic conditions ($\partial\theta/\partial X=0$) are used for the vertical walls, and hot and cold wall temperatures are taken as 1 and 0, respectively. At the inlet U=1, V=0, and θ=-0.5. At the exit port of the cavity, a uniform fluid temperature and uniform flow are assumed ($\partial\Phi/\partial X=0$ and $\partial\Phi/\partial Y=0$), where Φ is any of the fluid properties such as velocity and temperature.

4 | Numerical Solution of Governing Equations

The governing equations were iteratively solved by the finite-volume method using Patankar's SIMPLE algorithm [10]. A two-dimensional, uniformly spaced, staggered grid system was used. The power-law scheme was utilized for the convective terms. The generalized equations resulting from the finite volume discretization will be of the form.

$$a_P\Phi_P=a_E\Phi_E+a_W\Phi_W+a_N\Phi_N+a_S\Phi_S+b=\sum a_{nb}\Phi_{nb}+b, \quad (8)$$

where, $a_P=a_E+a_W+a_N+a_S+a_0$.

In the present formulation, the computational domain was divided into control volumes such that the control volume faces fall on the boundary of the square body. The equations are solved in the fluid and the solid regions simultaneously with suitable modifications. In the fluid region, the momentum equations are solved as usual, and when the solid medium is reached, the velocities in the solid region are set to zero. The matching conditions at the solid/fluid interface are also simultaneously satisfied. The algorithm ensured the continuity of fluxes at all control surfaces. The abrupt changes in the thermal conductivity are dealt with using the harmonic mean formulation as suggested in Patankar [10].

$$k_{bs}=\frac{2k_sk_f}{k_s+k_f}. \quad (9)$$

The TDMA [10] is applied for the line-by-line solution of the momentum, energy, and pressure correction equations. The process is repeated until the criteria of convergence for the continuity equation, which is less

than 10-6, are satisfied. For the thermal boundary condition, the process is repeated until the criterion of convergence $(\theta^{new} - \theta^{old}) / \theta^{new} \leq 10^{-5}$ is satisfied for temperature. For Re numbers other than 500 or Richardson numbers other than 10, the under-relaxation parameters for u, v, and T are all set to 0.5, whereas the under-relaxation parameter for pressure correction is set to 0.3. For Re = 500 and Ri=10, these parameters for u and v were set to 0.3. Patankar

4.1 | Grid Independence Study

In order to determine the proper grid size for this study, a grid independence test was conducted with Re = 300, Ri = 10, and s = 0.5. Five uniformly spaced grid densities were used for the grid independence study. These grid densities were $30^x \times 30^y$, $42^x \times 42^y$ and $60^x \times 60^y$, $75^x \times 75^y$, $90^x \times 90^y$. The mean Nusselt number at the hot wall is commonly used as a sensitivity measure of the accuracy of the solution and was selected as the monitoring variable for the grid independence study. *Fig. 2* shows the dependence of the quantity $\overline{Nu}_h$ on the grid size, from which it is observed that there is an insignificant change beyond a $60^x \times 60^y$ grid size. Therefore, considering both the accuracy and the computational time, the following calculations were all performed with this grid system.

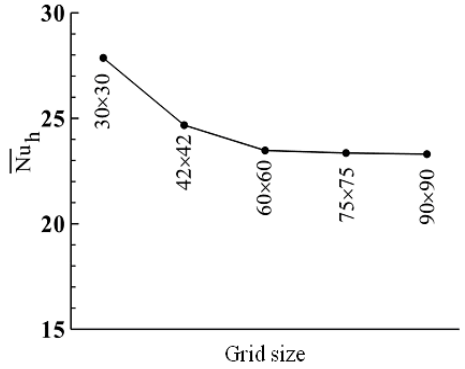

Fig. 2. The value of the mean Nusselt number, as a function of the grid size (Re = 300, Ri = 10, and s = 0.5).

4.2 | Code Validation

A test for validation of this numerical method was performed by simulating two similar models [11], [12] and is shown in *Tables 2* and *3*. It is seen that the present numerical solutions fairly agree with the results in the references. For the first case, a forced convection in a square cavity with inlet and outlet ports was solved. The comparison of the average Nusselt number is shown in *Table 2* for s=2.125. For the other one, a natural convection in a square cavity with a heat-generating conducting body was simulated. *Table 3* shows the comparison of the average Nusselt number at the hot bottom wall. The results show a good agreement.

Table 2. Comparison of $\overline{Nu}$ for validation at s=2.125.

Re	10	40	100	500
Present	4.072	7.038	9.936	20.433
Ref [10]	4.107	6.962	9.787	19.910

Table 3. Comparison of $\overline{Nu_h}$ for validation at k=0.1 and ΔT=0.

Ra	10^3	10^4	10^5	10^6
Present	0.823	2.325	3.843	5.947
Ref [11]	0.798	2.322	3.886	6.235

5 | Results and Discussion

In order to understand the flow field and heat transfer characteristics of this problem, a total of 36 cases were considered. This involved studying the effect of placing an outlet port at three different positions for a fixed position of the inlet port. The working fluid was chosen as air, with Pr=0.7. The governing parameter in this problem is the Richardson number, $Ri = Gr/Re^2$, which characterizes the relative importance of buoyancy to forced convection. For each configuration, the Reynolds number was selected to be 20, 100, and 300. For each value of Re, the Richardson numbers, Ri, were varied from 0 to 10, encompassing a range of dominating forced convection to dominating natural convection. The comparison among different configurations for efficient cooling is done based on the maximum temperature of the body and the average Nusselt number at the hot and cold walls. For effective cooling, the maximum temperature of the body and the average Nusselt number at the hot wall should be lower, while the average Nusselt number at the cold wall should be higher. Due to the interaction of the forced and natural convection, the analysis of the complex mixed-convection flow in the cavity is difficult. Intuitive inferences are sometimes contrary to reality. Nevertheless, the flow and thermal fields for all simulations were closely scrutinized, since it is not possible to include the results for all the configurations at all Re and Ri due to space limitations. Some representative streamlines and isotherms are shown for all the configurations at various Re and Ri in *Figs. 3-5*.

5.1 | Flow and Thermal Fields in the Cavity

Fig. 3 shows the flow and thermal field for configuration I (fluid exit from the top of the left wall) in terms of the streamlines and isotherms. The streamlines describe the interaction of forced and natural convection under various convection regimes. At low Reynolds number, for Ri < 1, forced convection dominates, and the major flow is diagonal from the inlet to the exit. At higher Re, recirculation zones are formed above the inlet port and heat-generating body. This zone above the inlet and body has a counterclockwise and clockwise direction, respectively. There is hardly any distortion in the flow streams until the buoyancy and inertia forces become equally dominant at Ri=1. For Ri>1, the buoyancy effects dominate, and the flow between the solid body and the cold wall forms a large recirculation zone at lower Re, whereas at higher Re, this is divided into more zones. Increasing the Richardson number has a low effect on the flow field around the hot bottom wall, because this wall is near the injection port, where the inertia force dominates. For high Reynolds and low Richardson numbers, there is a clockwise vortex at the right corner of the bottom of the cavity and above the solid body, where, with increasing Richardson numbers, this zone disappears. The thermal field is governed more or less by the interaction between the incoming cold fluid stream and the circulating vortex.

It also depends on where the vortex is created inside the cavity. The high-temperature circulating region is more concentrated near the heat-generating conducting body, where there is a large temperature gradient under it. That is because the cold flow passes from that area, and high heat transfer happens there. For any value of Ri, increasing Re, filling the cavity with cold fluid, causes the maximum temperature of the solid body to decrease, where it leads to a higher temperature gradient close to the hot wall. It is observed that an increase in Richardson number increases the temperature of these regions, which is because these zones prevent the incoming cold air from flowing into this area. For a high Richardson number (10), an increase in Reynolds number increases interaction between the incoming cold fluid stream and the circulating vortex, decreasing the temperature of these zones and the solid body. Both isotherms and streamlines for Ri =10 show that the hot fluid stream rises vertically from the solid body to the cold wall. That is because increasing the Richardson number increases the buoyancy force.

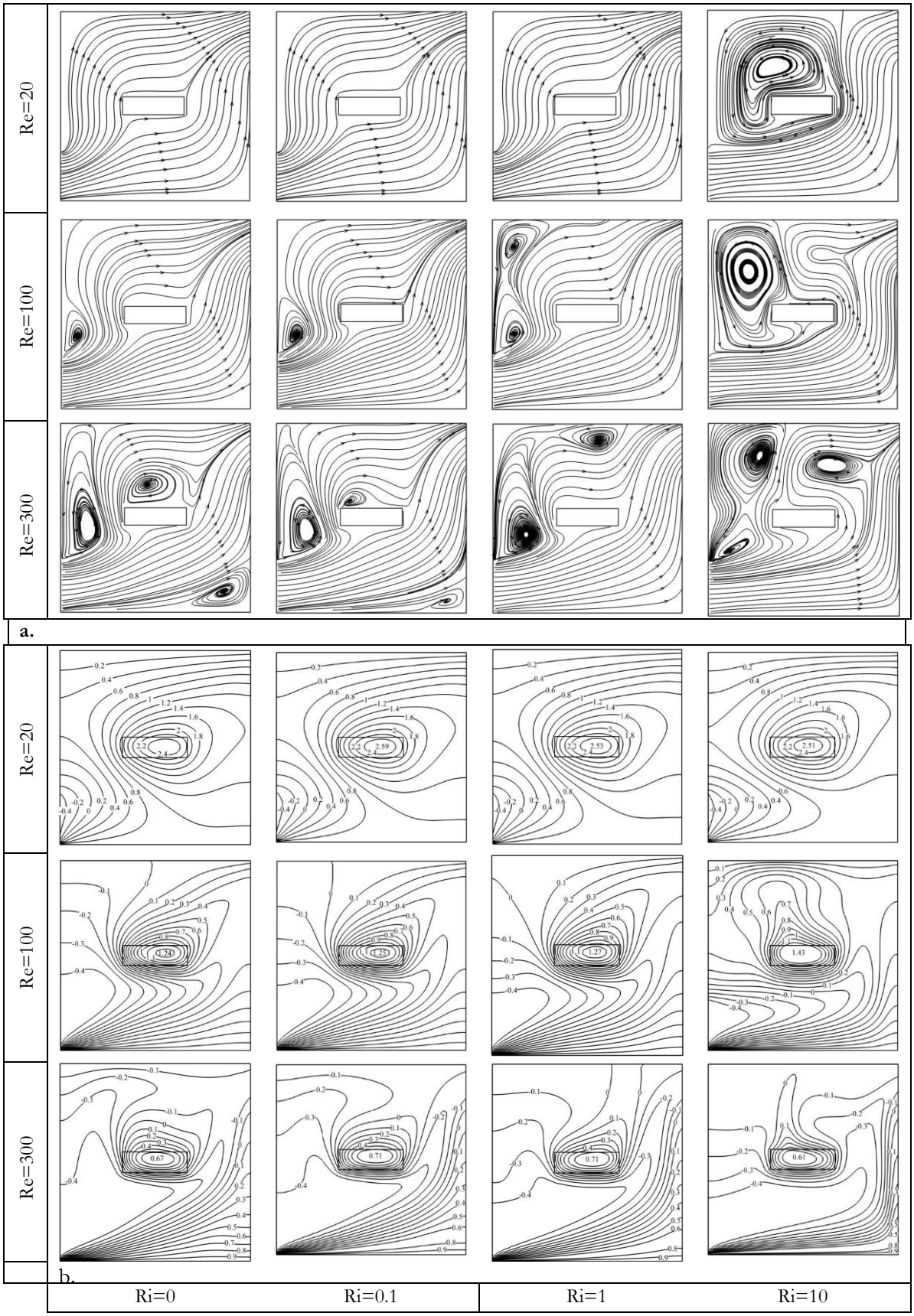

Fig. 3. Streamlines; a. isotherms, and b. for configuration I.

Fig. 4 shows the streamlines and isotherms for configuration II (fluid exit from the middle of the left wall). For low Reynolds number and Ri ≤ 1, forced convection dominates, and the major flow is diagonal from the

inlet to the exit. At a higher Ri (10), a counterclockwise recirculation zone is formed around the heat-generating body. For higher Re, recirculation zones are formed above the inlet port, similar to configuration I. Large recirculation zones in the cavity are developed at higher Re and Ri. In this case, the interaction between the incoming cold fluid stream and the circulating vortex becomes less toward the configuration I. Here, for a high Reynolds number, there are other recirculation zones at the top of the right corner of the cavity. As shown in Figure 4 for isotherms, the variations of Reynolds and Richardson numbers have similar effects on the thermal field, such as configuration I. It is noticed that in this case, the region above the body has a higher temperature than the similar region in configuration I and so this area has lower temperature gradients.

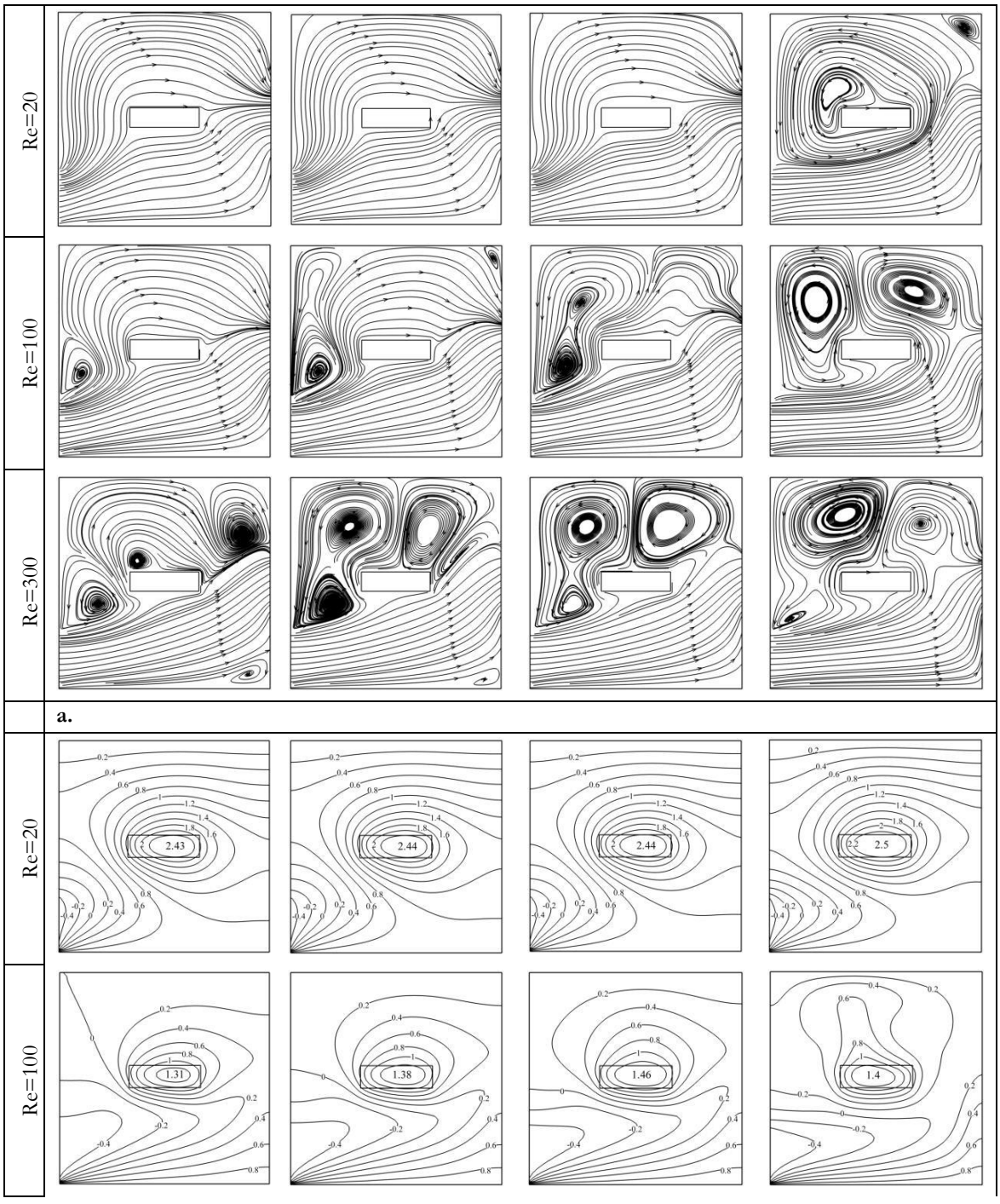

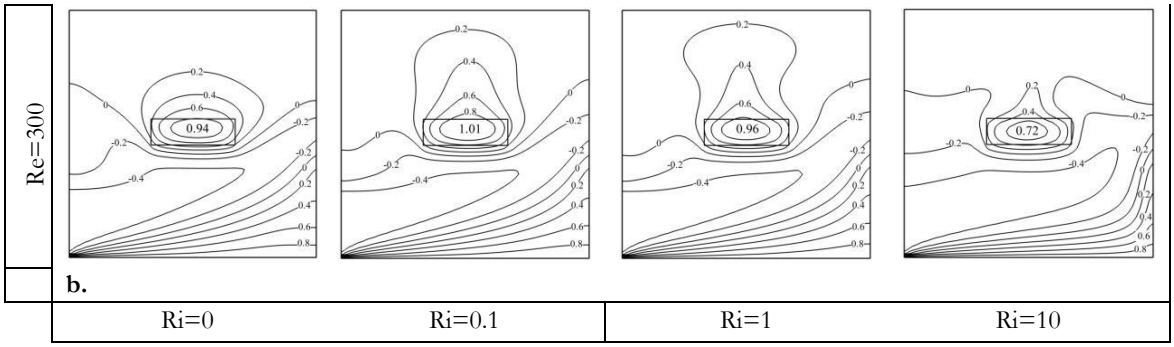

Fig. 4. Streamlines; a. isotherms, and b. for configuration II.

Fig. 5 shows the flow and thermal field for configuration III (fluid exit from the bottom of the left wall). In this case, there are two separate stream zones, one stream flowing from inlet to outlet without any distortion, and the other is made of some circulating vortex around the solid body. So, recirculation zones have no contact with the incoming cold air jet except for low Reynolds numbers. For high Reynolds numbers, increasing. Richardson number bifurcates a large recirculation zone with two reverse directions. For Ri =10, a hot fluid stream rises vertically from the middle of the solid body to the cold wall, which it makes two equally vortex zones. Here, variations of Re and Ri have similar effects on the thermal field, as in other cases. It is strongly observed that configuration III has the most temperature gradients at the hot bottom wall. The reason is that, in this case, the hot wall is between the inlet and outlet ports, which forces a great heat transfer to the cold air.

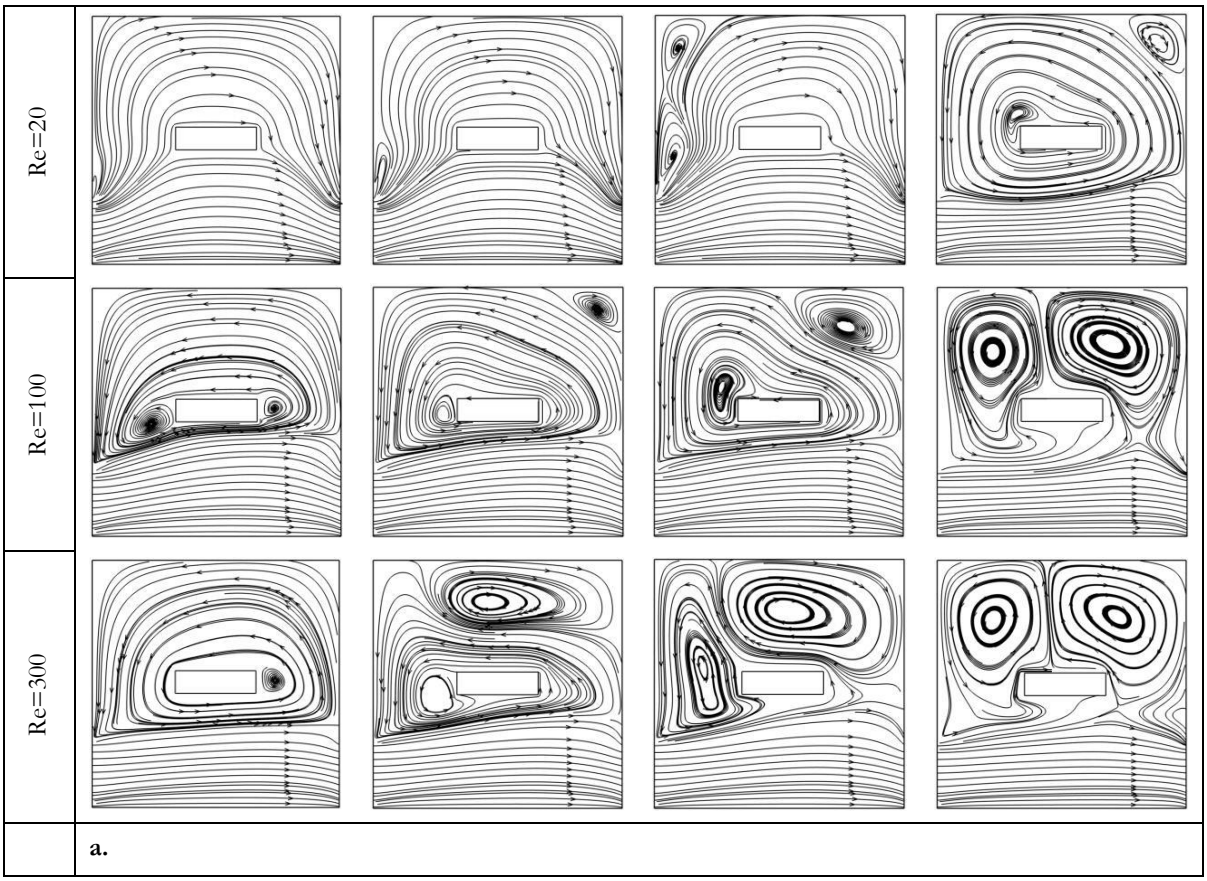

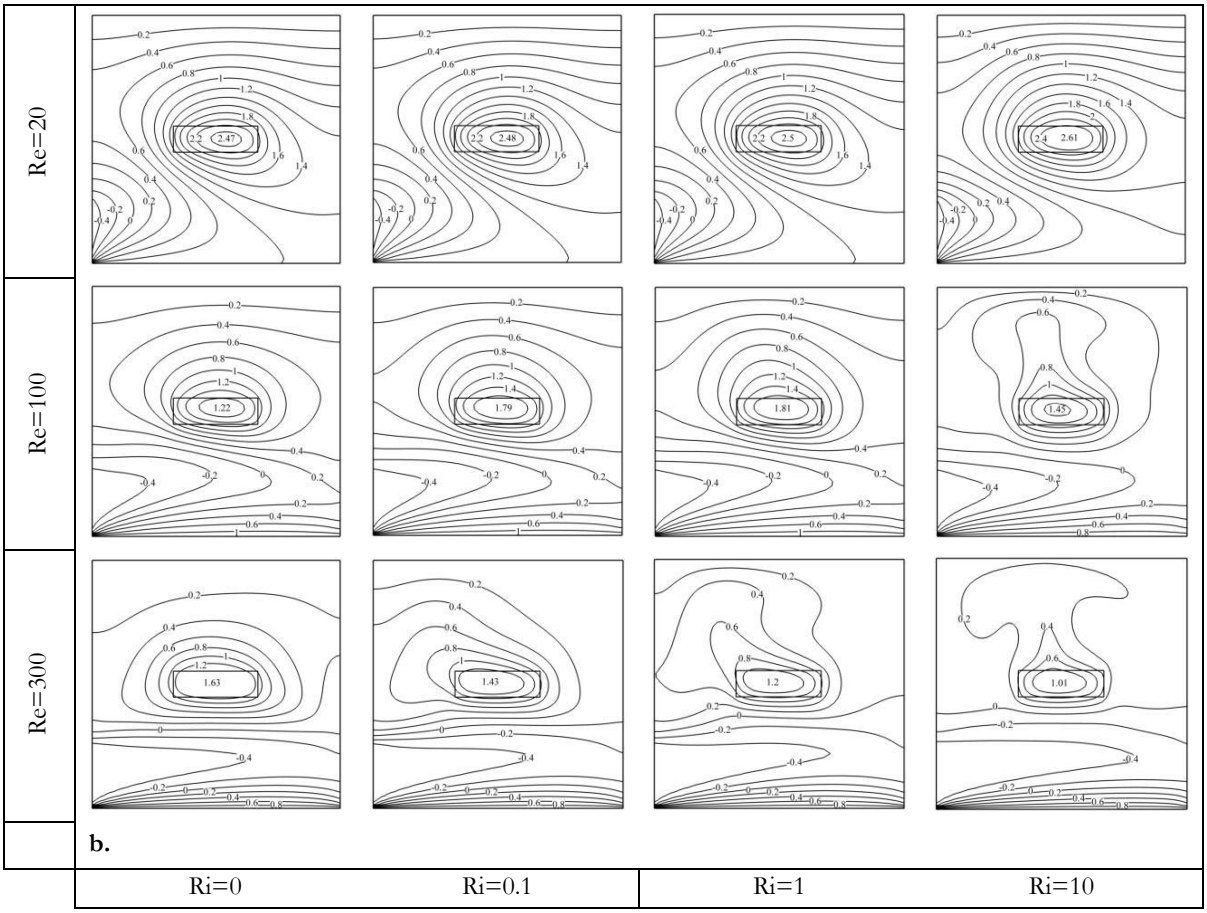

Fig. 5. Streamlines; a. isotherms, and b. for configuration III.

Fig. 6 shows variations of maximum temperature in the solid body (θmax) with Richardson number, for three configurations and various values of Reynolds numbers. The figure shows that, for higher Reynolds numbers, θmax becomes lower, which is because an increase in Reynolds number results in the cavity filling with more cold fluid, causing the maximum temperature of the solid body to decrease. Comparing these graphs together, represent that for each Reynolds number for configuration I and for s=0.875, the maximum temperature of the solid body is lower. As mentioned above, in this case, the major flow is diagonal from the inlet to the outlet. Therefore, the vorticity regions around the body decrease, and the hot body comes into better contact with the incoming cold air jet where its temperature decreases.

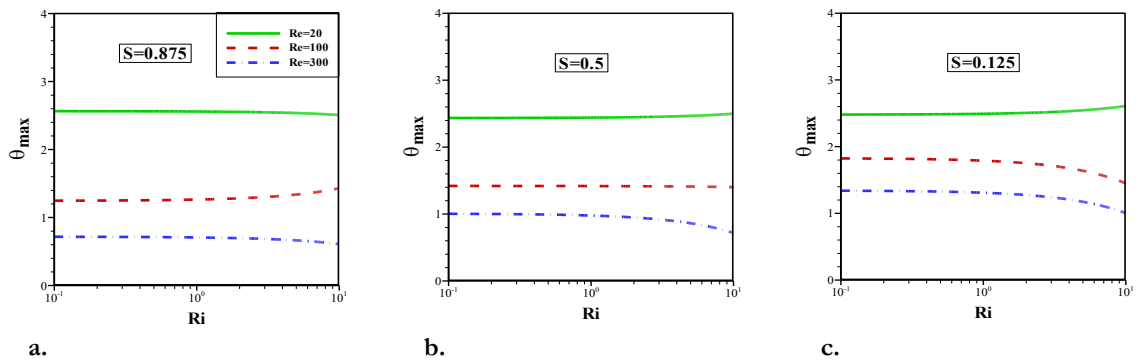

Fig. 6. Variations of maximum temperature in solid body (θmax).

5.2 | Variation of Nusselt Number at Isotherm Walls

In order to evaluate the heat transfer rate along the walls, it is necessary to observe the variations of the local Nusselt number on these walls. These are defined as

$$\mathrm{Nu}_i = -\left.\frac{\partial\theta}{\partial y}\right|_{\mathrm{wall}} . \tag{10}$$

With the subscript i representing c and h that correspond to the top and bottom walls, respectively. Variations of the local Nusselt number on the hot and cold walls for three configurations and various values of Reynolds and Richardson numbers are shown in *Figs. 7* through *8*, respectively.

Fig. 7 indicates that the local Nusselt number at the hot bottom wall, Nu_h, becomes increasingly flattened with x. At x=0, the cold flow enters the cavity and the difference between its temperature and the hot wall temperature, Th, is maximum, where, far from the inlet, this difference becomes less. Therefore, increasing x decreases the heat transfer rate and so the Nusselt number. As mentioned before, variation of the Richardson number does not affect obviously on the Nusselt number at the hot wall.

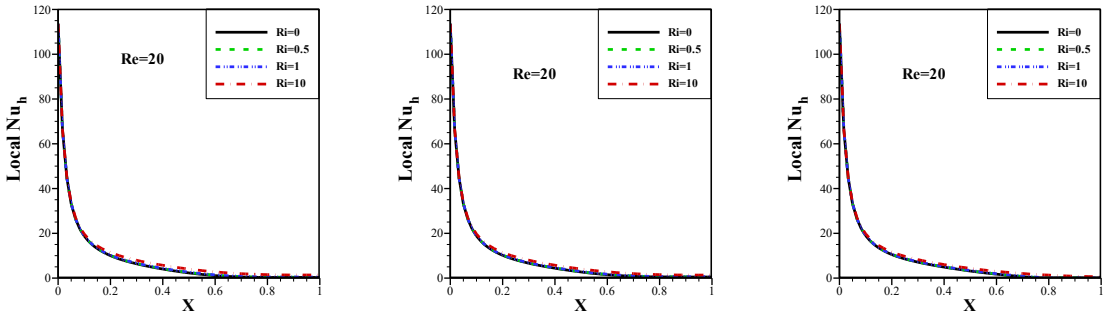

a.

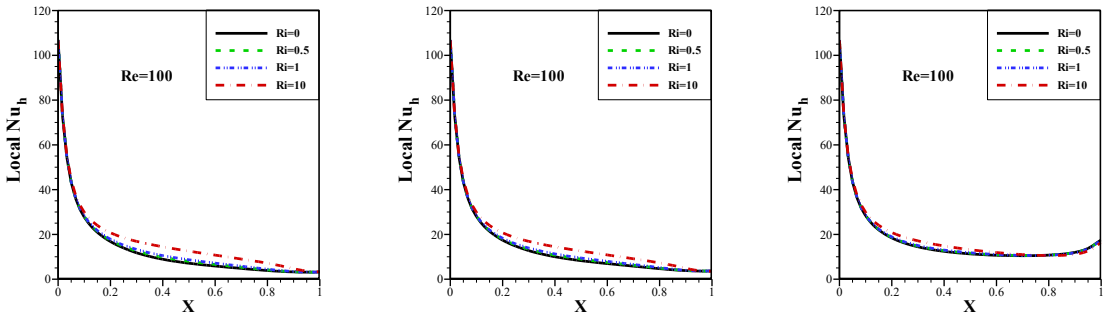

b.

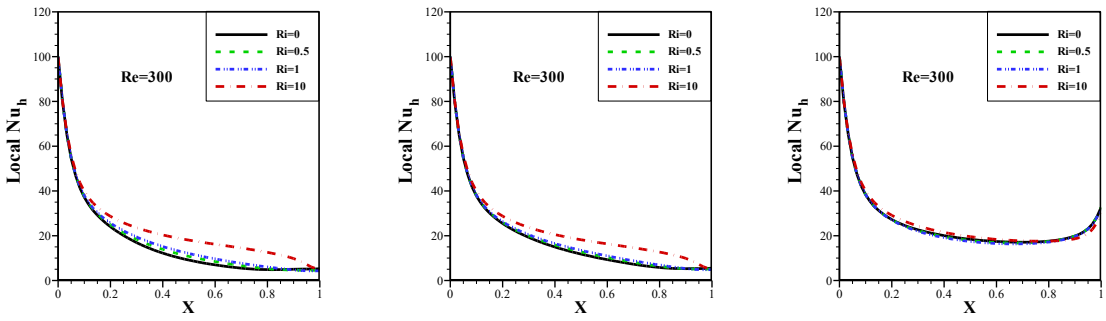

c.

Configuration I Configuration II Configuration III

Fig. 7. Variations of local Nusselt number at the hot wall.

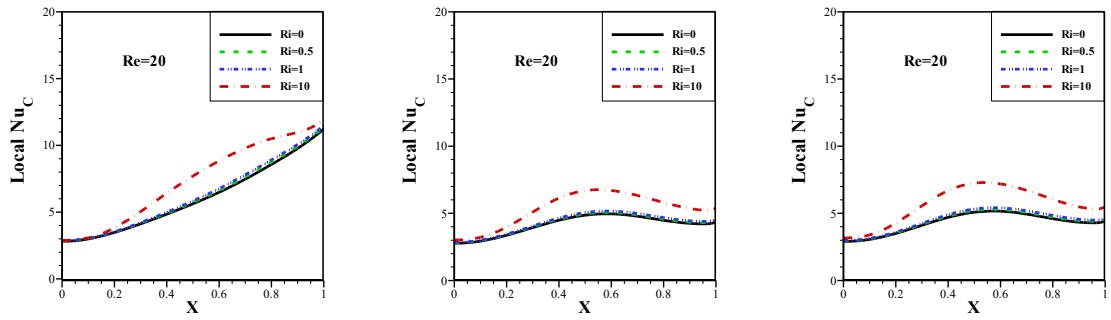

a.

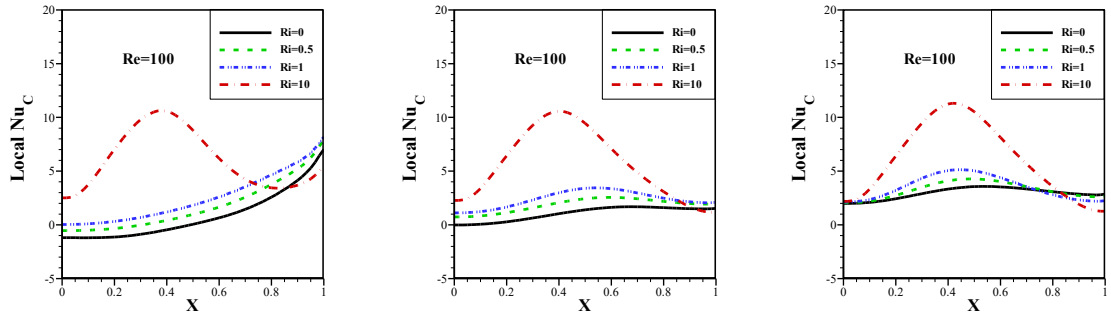

b.

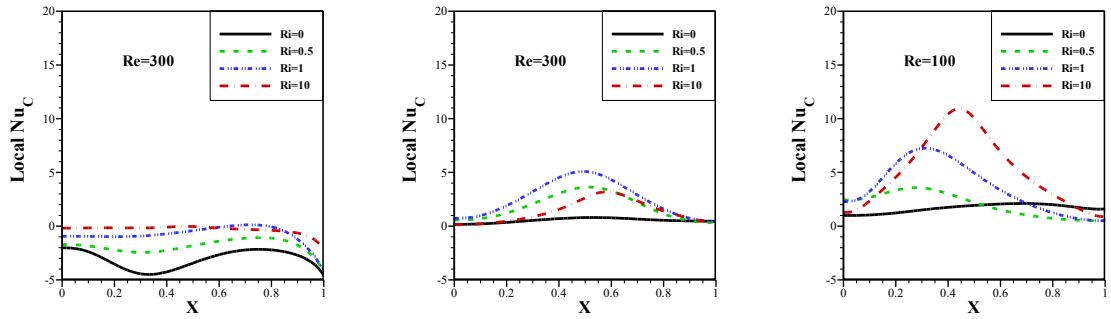

c.

Configuration I Configuration II Configuration III

Fig. 8. Variations of local Nusselt number at the cold wall.

Fig. 8 indicates that increasing x increases the local Nusselt number at the cold wall. That is because the incoming flow becomes warm, increases the difference between flow temperature and Tc, causing an increase in the Nusselt number. In some graphs, there is a peak value for a high Richardson number. As shown in streamlines, for high Ri, the hot fluid stream rises vertically from the middle of the solid body to the cold wall, where it makes two equally vortex zones.

Therefore, in that area, the temperature of fluid increases and the difference of T and Tc becomes, causing an increase in the Nusselt number for that zone. For configuration I for high Reynolds number, somewhere the value of the Nusselt number becomes negative. An increase in Re causes an increase in incoming cold air flow rate, where the fluid temperature in those zones becomes lower than Tc. Another variable utilized to

evaluate the heat transfer rate is the overall or average Nusselt number of the cavity. The average Nusselt number is defined as

$$\overline{Nu} = \frac{1}{L}\int_0^L Nu\, dL. \tag{11}$$

The average Nusselt number of the hot and cold walls as a function of the Ri number, for different Re numbers and three configurations, is given in *Fig. 9*. Results show that with an increase in Reynolds number, the average Nusselt number for the hot wall $\overline{Nu}_h$ increases, while the average Nusselt number for the cold wall $\overline{Nu}_c$ decreases. The results show that increasing the Richardson number increases the Nusselt number, which is due to increasing inertia forces and natural convection.

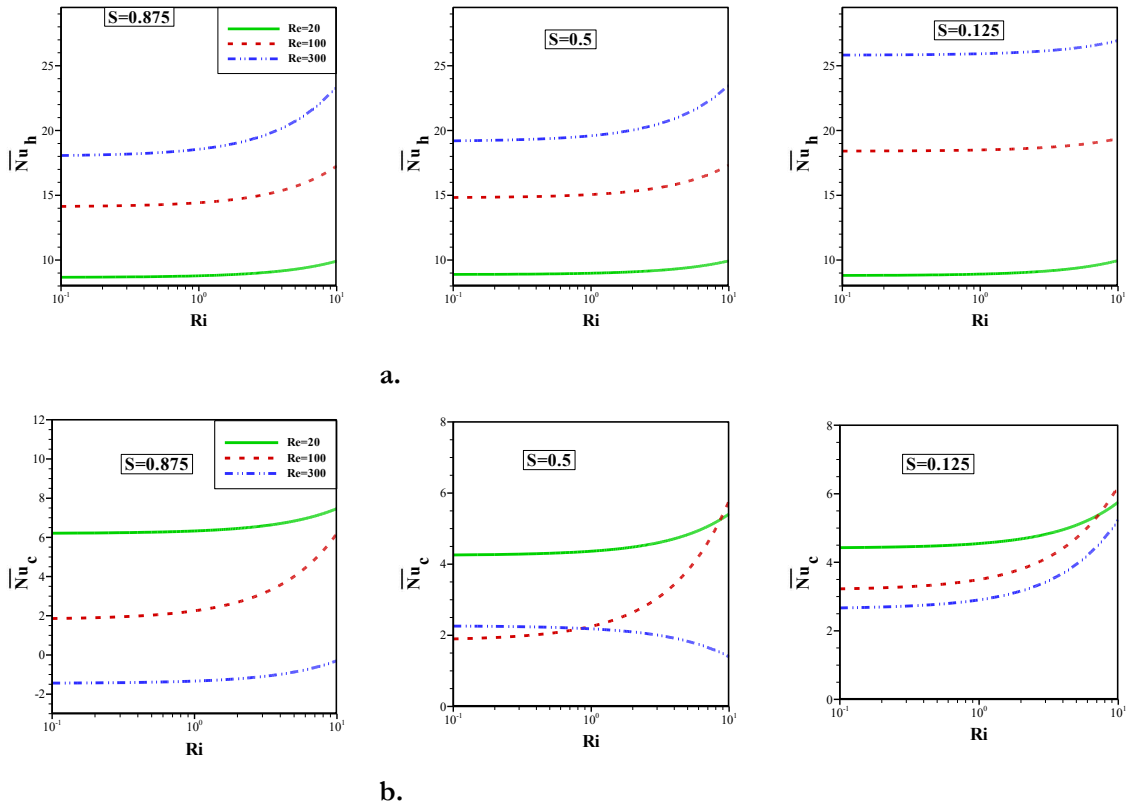

Fig. 9. Variations of average Nusselt number at the; a. hot wall, and b. cold wall.

6 | Conclusion

A numerical investigation of a laminar mixed-convection in a square cavity with a heat-generating conducting body has been conducted to identify the optimum placement of the exit port through the right wall for best cooling effectiveness. A total of three outlet placement configurations have been considered. The maximum temperature in the heat-generating body (θmax) has been used to compare the cooling effectiveness among different configurations. Results show that in configuration I (when the exit port is located at the top of the right wall), cooling of the heat-generating body is optimum.

In this configuration, the solid body is situated on the genuine route of the fluid flow, from the inlet to the outlet. In this case, the vorticity regions around the body decrease, where the hot body comes into better contact with the incoming cold air jet, decreasing its temperature. It is also observed that, with an increase in Richardson number, the buoyancy effects dominate, and the flow between the solid body and the cold wall forms a large recirculation zone, where it may increase the solid body temperature. Using configuration I, it may avoid isolated recirculation zones carrying hot fluid.

Funding

No funding was received for conducting this study.

Data Availability

All data are included in the text.

Conflicts of Interest

The authors declare no competing interests.

References

[1] Papanicolaou, E., & Jaluria, Y. (1991). Mixed convection from an isolated heat source in a rectangular enclosure. *Numerical heat transfer*, *18*(4), 427–461. https://doi.org/10.1080/10407789008944802

[2] Karki, K. C., Sathyamurthy, P. S., & Patankar, S. V. (1992). Natural convection in a partitioned cubic enclosure. *Journal of heat transfer*, *114*(2), 410–417. https://doi.org/10.1115/1.2911289

[3] Prasad, A. K., & Koseff, J. R. (1996). Combined forced and natural convection heat transfer in a deep lid-driven cavity flow. *International journal of heat and fluid flow*, *17*(5), 460–467. https://doi.org/10.1016/0142-727X(96)00054-9

[4] Hsu, T. H., Hsu, P. T., & How, S. P. (1997). Mixed convection in a partially divided rectangular enclosure. *Numerical heat transfer, part a applications*, *31*(6), 655–683. https://doi.org/10.1080/10407789708914058

[5] Lee, S. C., Cheng, C. Y., & Chen, C. K. (1997). Finite element solutions of laminar and turbulent flows with forced and mixed convection in an air-cooled room. *Numerical heat transfer, part a applications*, *31*(5), 529–550. https://doi.org/10.1080/10407789708914051

[6] Singh, S., & Sharif, M. A. R. (2003). Mixed convective cooling of a rectangular cavity with inlet and exit openings on differentially heated side walls. *Numerical heat transfer: part a: Applications*, *44*(3), 233–253. https://doi.org/10.1080/716100509

[7] Omri, A., & Nasrallah, S. Ben. (1999). Control volume finite element numerical simulation of mixed convection in an air-cooled cavity. *Numerical heat transfer: Part a: Applications*, *36*(6), 615–637. https://doi.org/10.1080/104077899274606

[8] Hsu, T. H., & Ang, S. G. W. (2000). Mixed convection in a rectangular enclosure with discrete heat sources. *Numerical heat transfer: part a: applications*, *38*(6), 627–652. https://doi.org/10.1080/104077800750021170

[9] Lee, J. R., Ha, M. Y., Balachandar, S., Yoon, H. S., & Lee, S. S. (2004). Natural convection in a horizontal layer of fluid with a periodic array of square cylinders in the interior. *Physics of fluids*, *16*(4), 1097–1117. https://doi.org/10.1063/1.1649989

[10] Patankar, S. (2018). *Numerical heat transfer and fluid flow*. CRC press. https://doi.org/10.1201/9781482234213

[11] Saeidi, S. M., & Khodadadi, J. M. (2006). Forced convection in a square cavity with inlet and outlet ports. *International journal of heat and mass transfer*, *49*(11–12), 1896–1906. https://doi.org/10.1016/j.ijheatmasstransfer.2005.10.033

[12] Lee, J. R., & Ha, M. Y. (2006). Numerical simulation of natural convection in a horizontal enclosure with a heat-generating conducting body. *International journal of heat and mass transfer*, *49*(15–16), 2684–2702. https://doi.org/10.1016/j.ijheatmasstransfer.2006.01.010

Appendix A

Nomenclature

A	Area ratio $A = \frac{WP}{L^2}$
g	Gravitational acceleration $\left(ms^{-2}\right)$
K	Dimensionless thermal conductivity (k_s/k_f)
L	Length of the enclosure
Nu	Local Nusselt number
Nu	Surface-averaged Nusselt number
$\overline{Nu}$	Local Nusselt number
P	Dimensionless pressure
Pr	Prandtl number
$\dot{q}$	Heat generation per unit surface
Re	Reynolds number
Ri	Richardson number
v, u	Velocity components in the x and y directions, respectively (ms^{-1})
Y, X	Dimensionless coordinate system
y, x	Coordinate system
T	Temperature (K)
Greeks	
α	Thermal diffusivity
β	Thermal expansion coefficient
ρ	Density of fluid (Kgm^{-3})
θ	Dimensionless temperature

List of tables

List of figures